AGU PUBLICATIONS

JGR

Journal of Geophysical Research: Solid Earth

RESEARCH ARTICLE

10.1002/2013JB010817

Special Section:
Stress, Strain and Mass Changes at Volcanoes

Modeling shear wave splitting due to stress-induced anisotropy, with an application to Mount Asama Volcano, Japan

Adrian Shelley[1], Martha Savage[1], Charles Williams[2], Yosuke Aoki[3], and Boris Gurevich[4]

[1]SGEES, Victoria University of Wellington, Wellington, New Zealand, [2]GNS Science, Lower Hutt, New Zealand, [3]Earthquake Research Institute, Tokyo University, Tokyo, Japan, [4]Department of Exploration Geophysics, Curtin University of Technology, Perth, Australia

Key Points:
- A forward model for stress-induced anisotropy in the crust was developed
- The model is applied to data for the 2004 eruption of Mount Asama, Japan
- Modeled anisotropy is small for deviatoric stress due to an inflating dyke

Correspondence to:
A. F. Shelley,
adrian.shelley@vuw.ac.nz

Citation:
Shelley, A., M. Savage, C. Williams, Y. Aoki, and B. Gurevich (2014), Modeling shear wave splitting due to stress-induced anisotropy, with an application to Mount Asama Volcano, Japan, *J. Geophys. Res. Solid Earth*, *119*, 4269–4286, doi:10.1002/2013JB010817.

Received 31 OCT 2013
Accepted 24 MAR 2014
Accepted article online 30 MAR 2014
Published online 13 MAY 2014

Abstract We use numerical modeling to investigate the proposed stress-based origin for changing anisotropy at Mount Asama Volcano, Japan. Stress-induced anisotropy occurs when deviatoric stress conditions are applied to rocks which are permeated by microcracks and compliant pore space, leading to an anisotropic distribution of open crack features. Changes to the local stress field around volcanoes can thus affect the anisotropy of the region. The 2004 eruption of Mount Asama Volcano coincided with time-varying shear wave splitting measurements, revealing changes in anisotropy that were attributed to stress changes associated with the eruption. To test this assertion, we create a model that incorporates knowledge of the volcanic stress, ray tracing, and estimation of the anisotropy to produce synthetic shear wave splitting results using a dyke stress model. Anisotropy is calculated in two ways, by considering a basic case of having uniform crack density and a case where the strength of anisotropy is related to dry crack closure from deviatoric stress. Our results show that this approach is sensitive to crack density, crack compliance, and the regional stress field, all of which are poorly constrained parameters. In the case of dry crack closure, results show that modeled stress conditions produce a much smaller degree of anisotropy than indicated by measurements. We propose that the source of anisotropy changes at Asama is tied to more complex processes that may precipitate from stress changes or other volcanic processes, such as the movement of pore fluid.

1. Introduction

Seismic anisotropy is increasingly being used as a geophysical tool to investigate the Earth's interior. Differential stress in the upper crust can create anisotropy through the closure of aligned cracks and mechanical discontinuities present in the rock mass [*Nur and Simmons*, 1969; *Crampin*, 1994]. This relationship provides a convenient way to monitor stress orientations in the crust, especially when there is a lack of geodetic observations (GPS, interferometric synthetic aperture radar, etc.) and studies of earthquake focal mechanisms are untenable. Possible changes in seismic anisotropy linked to volcanic activity associated with relatively short-term (days to years) magmatic processes [e.g., *Jónsson*, 2009] have been investigated as more complete data sets are collected [*Savage et al.*, 1990; *Munson et al.*, 1995; *Bianco et al.*, 1998; *Gerst and Savage*, 2004; *Savage et al.*, 2010; *Johnson et al.*, 2010]. However, there have been few quantitative studies on the effect of stress on in situ anisotropy measurements. Understanding of how anisotropy around volcanoes changes over time provides a potential tool for forecasting volcanic activity and in addition will provide insight into the role of stress-induced anisotropy in the upper crust.

We use computer modeling to investigate how changing stress conditions may affect crack-induced anisotropy. To do this, we model shear wave splitting in earthquakes using the interaction between crack-induced anisotropy and stress conditions during the 2004 eruptive episode at Mount Asama Volcano, Japan, and compare the results with shear wave splitting measurements made by *Savage et al.* [2010]. We also demonstrate the application of the analytical relationship between stress and elastic anisotropy proposed by *Gurevich et al.* [2011] to the three-dimensional stress and ray path model. Future models can potentially incorporate other analytical or empirical stress-anisotropy relationships. Forward modeling of the effect of anisotropy on shear waves is carried out using a method adapted from that used by *Abt and Fischer* [2008], described later.

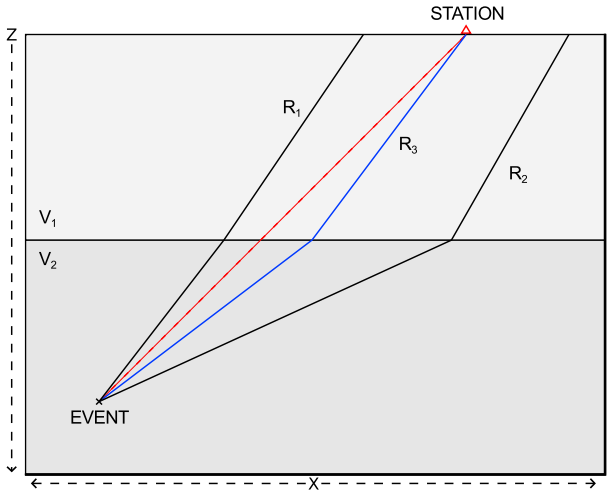

Figure 1. The red dashed line is the earthquake to station distance. Three rays are traced with successively increasing incident angles with respect to the event. R_1 is projected, and the ray destination is closer to the event than the station. The incidence angle is increased, the result being R_2, whose destination is further away than the station. At this point incidence angles in between R_1 and R_2 are projected until ray R_3 is found, whose destination is suitably close to the destination station.

Seismic anisotropy arises from the presence of discontinuities, crystal-preferred orientations, and material heterogeneities in rocks. These types of features are all present in the brittle upper crust [e.g., *Godfrey et al.*, 2000]; however, over the relatively short time periods over which volcanic activity occurs we do not expect any significant reorientation of crystal lattices or redistribution of rock material. The mechanical nature of discontinuities, however, has been shown to respond rapidly to the application of a nonuniform stress [*Zatsepin and Crampin*, 1997]. Small-scale discontinuities, such as cracks and grain contacts (microcracks), preferentially close relative to their alignment normal to the maximum compressive stress direction, so that the distribution of microcracks in terms of their effect on the overall elastic properties of the rock mass becomes anisotropic. This means that, as long as there is a degree of differential stress, particle motion parallel to the direction of maximum compressive stress is mechanically less impaired than orthogonal particle motion, resulting in higher velocities [*Babuška and Cara*, 1991]. In the case of shear waves, velocities in an anisotropic medium vary depending on their polarization. Measuring the direction of the fast polarization and the delay time from earthquake *S* waves provides information on the orientation and strength of anisotropy present in the rock medium that the ray passed through. Microcracks are generally assumed to be randomly oriented and thus isotropically distributed over macroscopic scales, as opposed to large-scale discontinuities (fractures) that tend to be in aligned sets. This is due to the nature of the microcracks being created during deposition (in the case of grain contacts in sedimentary rocks) or postrock formation after initial high temperature and pressure conditions are lifted [*Walsh*, 1965], rather than large-scale fractures which occur due to more consistent tectonic forces.

There is an inherent ambiguity when analyzing changes in anisotropy measurements from earthquake-generated waves, as it is hard to determine whether changes can be attributed to temporally evolving conditions or to effects dependent on path or source conditions [e.g., *Zinke and Zoback*, 2000; *Johnson et al.*, 2011]. There may only be a relatively short period of time during which magma body inflation or deflation is occurring, limiting the number of available seismic events that sample these transient stress states. This makes distinguishing between temporal and spatial changes in anisotropy vital to attain a robust interpretation of data. In order to predict the spatial component of anisotropy expected to coincide with volcanic activity, Coulomb stress modeling has been used as an aid for comparative interpretation between measurements and the assumed stress field [*Savage et al.*, 2010; *Johnson et al.*, 2011; *Roman et al.*, 2011]. Two-dimensional tomography [*Johnson et al.*, 2011] has also been implemented; however, there is a comparative lack of three-dimensional models looking at stress-induced anisotropy in the crust and around volcanoes. A three-dimensional model will provide the potential to take into account not only the state of stress as it changes vertically and laterally but also the propagation direction of the ray and the stress contribution from loading. By modeling shear wave splitting caused by stress in three dimensions, the contribution made by stress-induced anisotropy can be further constrained in order to aid future interpretation of splitting measurements.

2. Method

The method we use is a combination of finite element method stress modeling and numerical evaluation of ray paths, anisotropy, and shear wave splitting. First, we create a number of stress models using a priori

Table 1. The One-Dimensional *S* Wave Velocity Structure (in ms^{-1}) That Was Used in the Model[a]

Z (km)	V_p	*Z* (km)	V_p
3	2471	−14	3558
2	2509	−15	3577
1	2661	−16	3588
0	2656	−17	3596
−1	2982	−18	3606
−2	3288	−19	3616
−3	3440	−20	3625
−4	3483	−21	3634
−5	3474	−22	3643
−6	3480	−23	3652
−7	3490	−24	3661
−8	3492	−25	3670
−9	3473	−26	3679
−10	3449	−27	3688
−11	3444	−28	3697
−12	3477	−29	3706
−13	3524	−30	3715

[a]*Z* denotes height above sea level. Density followed a simple linear relationship with depth from 2500 to 3000 kg m^{-3} from the top to the bottom of the model space.

knowledge about the region and the volcanic source, in this case an inflating dyke. Ray paths are then traced through the model space at which point various models and comparisons are performed. We look at stress-raypath interaction and calculate shear wave splitting along raypaths. The anisotropic elastic properties used to calculate shear wave splitting parameters are set along raypaths using the stress data and two different models from *Hudson* [1981] and *Gurevich et al.* [2011].

2.1. Stress Modeling

Stress changes are computed using the PyLith finite element code [*Aagaard et al.*, 2007, 2013], which was specifically designed for modeling crustal deformation. An important feature for our work is the ability to model faults and/or dykes. We do not include the effect of topography on gravitational stresses because we are only interested in relative changes in the stress state. The seismic velocities and densities used to calculate the elastic properties of the model are the same as in the one-dimensional model used to trace the seismic ray paths through the model, which will be detailed in the later section on ray tracing. PyLith allows for the modeling of the crustal volume using an elastic rheology, Dirichlet (displacement or velocity) boundary conditions, and kinematic fault interfaces that are applied to model various volcanic features. The dyke opening is modeled using kinematic fault conditions, in which along-strike displacement is set to zero and deformation is controlled using a plane-normal opening parameter. We model a background regional stress in all cases apart from those in which only the dyke stress, rather than the overall stress conditions, is needed. The parameters used for the dyke and for background stresses are outlined in sections 2.5 and 2.6, respectively. We apply fixed boundary conditions on all model faces other than the topographic surface.

The output is then regridded from a tetrahedral mesh to a regular cubic one at the desired resolution for input into the ray tracer and synthetic shear wave splitting code. We use both 1000 m and 500 m grid sizes for this resampling. The higher resolution 500 m grid size is used for all model results shown here. The stress data are averaged over each new grid element and the principal stress magnitudes (σ_1, σ_2, and σ_3), and corresponding direction cosines (three for each principal stress) are also calculated.

2.2. Seismic Ray Tracing

The model space for the ray tracing and subsequent anisotropy calculation consists of a three-dimensional ordered array of cubes, to which each are assigned uniform material properties. The resolution of the blocks governs the minimum resolvable features in the model. Model coordinates are normalized around the center of the dyke feature being modeled, with depths being measured relative to sea level.

A one-dimensional subsurface seismic velocity model is used to trace ray paths through the model space. *P* wave velocities around Asama inferred from an active source seismic experiment [*Aoki et al.*, 2009] are averaged over each depth and then interpolated to the specified model depth increments (see Table 1). *S* wave velocities are found assuming a V_p/V_s of 1.7, after *Savage et al.* [2010]). This velocity model is also used to constrain elastic data in the stress model. A further constraint about near-surface density at Asama is provided by cosmic ray muon radiography [*Tanaka et al.*, 2007]. For simplicity, we employ a one-dimensional density model that increases linearly with depth from 2500 kg m^{-3} at the surface to 3000 kg m^{-3} at 30 km below sea level.

Each ray path is traced through the model by finding incidence angles at set depth levels using the 1-D velocity model. This is achieved by iteratively evaluating successively finely spaced ray path angles until the path that has the station as the destination is found (see Figure 1). A common ray approximation, where each polarized shear wave follows the same ray path, is assumed throughout the model.

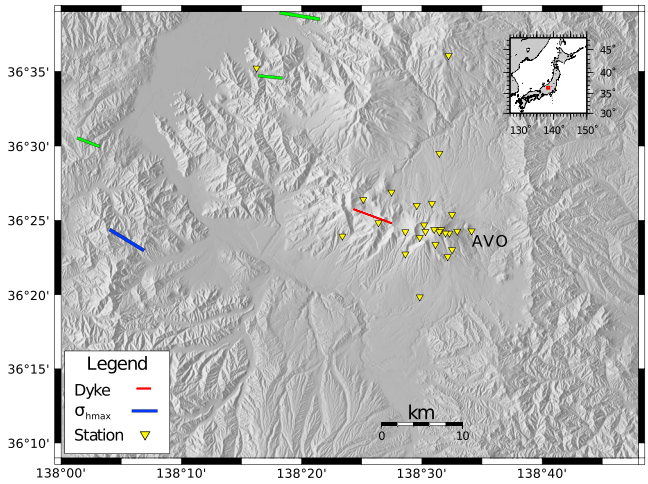

Figure 2. The Asama region in central Japan, showing S_{Hmax} directions determined from earthquake focal mechanisms by *Townend and Zoback* [2006]. Strike-slip and reverse stress states are shown in green and blue, respectively. Large symbols are measurements made from restricting the focal mechanism data to those with strike, dip, and rake uncertainties of $\leq 10°$, whereas small symbols represent measurements whose rake uncertainties are $> 10°$. Also shown is the regional seismic network situated around Asama, with station AVO indicated.

Regional events occurring beneath 30 km, outside the model space, are traced using the same technique at a lower resolution using the 1-D velocity/density model, AK135 [*Kennett et al.*, 1995], in order to find the location at which the ray path pierces the stress model boundary.

2.3. Stress and Anisotropy Calculations

We approach the subsequent modeling in three successive ways in order to investigate the influence of the magnitude and orientation of volcanic stress on anisotropy. First, we consider stress magnitudes in isolation in order to establish a measure of raypath-stress interaction. Second, we consider stress orientation in conjunction with an anisotropic model based on assumed crack densities as a basic approach to investigate the link between modeled stress orientations and measured fast directions, as well as crack density and measured delay times. Last, we look at the effect of both stress orientation and magnitude on modeled shear wave splitting.

Combining stress models and the traced ray paths allows us to quantify, for each ray, the range of stress magnitudes in the raypath vicinity due to dyke inflation. Under the assumption that stress is the source of anisotropy changes in the crust, it is useful to know to what degree the stress field is perturbed by volcanic sources for each raypath. Hypothetically, greater stress magnitudes from the dyke source would result in a more pronounced effect on shear wave splitting. In the simplest case of stress-induced anisotropy arising from crack closure (all else being equal), the magnitude of a stress perturbation in a volume should correlate well with the magnitude of anisotropy change. This analysis gives insight into stress interaction with raypaths which can then be compared with the shear wave splitting measurements to assess the relationship between the two.

To be able to model anisotropic effects on a shear wave, its medium's elastic properties must be calculated. *Hudson* [1981] provides first-order relationships between crack density (ϵ) and the stiffness tensor (C_{ijkl}) for a rock with an aligned set of circular cracks. These are valid at dilute crack concentrations ($\epsilon \ll 1$). They are characterized by the isotropic stiffness tensor, C^{iso}, defined by the rock's Lamé parameters, modified by some constant, C^{an}, such that

$$C_{ijkl} = C^{iso} + C^{an} \tag{1}$$

Due to its symmetry, the fourth-order elastic tensor can be defined as a second-order tensor (see Appendix A). For dry cracks, the nonzero elements of C^{an} are

$$C^{an}_{11} = C^{an}_{12} = C^{an}_{21} = C^{an}_{22} = -\frac{4}{3}(\epsilon)\frac{\lambda^2(\lambda+2\mu)}{\mu(\lambda+\mu)}$$

$$C^{an}_{13} = C^{an}_{31} = C^{an}_{32} = C^{an}_{23} = -\frac{4}{3}(\epsilon)\frac{\lambda(\lambda+2\mu)^2}{\mu(\lambda+\mu)}$$

$$C^{an}_{33} = -\frac{4}{3}(\epsilon)\frac{(\lambda+2\mu)^3}{\mu(\lambda+\mu)}$$

$$C^{an}_{44} = C^{an}_{55} = -\frac{32}{3}(\epsilon)\frac{\mu(\lambda+2\mu)}{(3\lambda+4\mu)}$$

where λ and μ are the Lamé parameters of the medium, and ϵ is crack density, or Na^3, with N being the number density of cracks and a being the mean crack radius. For fluid-filled cracks a different formulation for the C^{an} matrix is derived based on a model in which shear traction on the crack is zero and there is only displacement in the transverse direction [*Hudson*, 1981]. In this case, the nonzero elements of C^{an} are

$$C_{44}^{an} = C_{55}^{an} = -\frac{32}{3}(\epsilon)\mu\frac{\lambda + 2\mu}{3\lambda + 4\mu}$$

C_{ijkl} can then be calculated for a given ϵ using Lameé parameters derived from seismic velocity and density data. A number of models are created in which different values of ϵ, which are constant throughout the model space, are used.

Finally, we incorporate stress magnitude and orientation into the determination of the medium's elastic properties using the analytical relationship developed by *Gurevich et al.* [2011]. This differs from Hudson's method by calculating the perturbation from the isotropic rock state using stress magnitude as a scaling factor. It is assumed that all cracks are identical and can be described by their area and the ratio between their normal and tangential excess crack compliance. In this case, the underlying framework of determining crack-induced elastic anisotropy is the noninteractive approximation made by *Sayers and Kachang* [1995], which is based on the assumption that there are no stress interactions between cracks. The accuracy of this approximation holds only if the positions of the cracks are random, as the presence of cracks in some pattern of alignment will have an overall effect on the average stress field. The change in compliance due to the presence of cracks given by Sayers and Kachang's approach is

$$\Delta S_{ijkl} = \frac{1}{4}(\delta_{ik}\alpha_{jl} + \delta_{il}\alpha_{jk} + \delta_{jk}\alpha_{il} + \delta_{jl}\alpha_{ik}) + \beta_{ijkl} \tag{2}$$

where α_{ij} is a second-order tensor defined as

$$\alpha_{ij} = \frac{1}{V}\sum_r B_T^r n_i^r n_j^r S_r$$

And β_{ijkl} is a fourth-order tensor defined as

$$\beta_{ijkl} = \frac{1}{V}\sum_r (B_N^r - B_T^r) n_i^r n_j^r n_k^r n_l^r S_r$$

where B_N^r is the normal and B_T^r the shear crack compliance term for the rth crack in volume V, n_i^r is the ith component of the rth crack normal, and S_r is the crack area.

Gurevich et al. [2011] express the dependence of tensors α_{ij} and β_{ijkl} as a function of stress using the following relationship between stress and specific crack area, $s = \Sigma A^r/V$, at a given orientation:

$$s = s^0 \exp(\sigma_n/P_c) \tag{3}$$

where s^0 is the specific area of all cracks before any stress is applied, σ_n is the normal stress traction acting on the crack surface, and P_c is some characteristic pressure at which cracks will close. Substituting this relationship into formulation for tensors α_{ij} and β_{ijkl} gives solutions that provide the stress-dependent compliance tensor, S_{ijkl}. This tensor, containing five independent coefficients and thus having hexagonal symmetry, can be calculated using the isotropic rock compliance, the stress state, and the crack compliances. The corresponding stiffness tensor is the inverse of the compliance tensor.

There are several assumptions that have been made e motions by *Gurevich et al.* [2011]:

1. The rock is assumed be rheologically elastic, an assumption also used by the stress model. This assumption is more problematic when considering volcanic processes, as rocks surrounding magma chambers will undergo a degree of thermomechanical weakening, and studies have found that taking a viscoelastic approach to modeling rheology can significantly reduce the magma chamber pressures needed to match ground deformation when compared to elastic models [e.g., *Newman et al.*, 2006; *Del Negro et al.*, 2009]. Stress may also cause failure in rocks, and even in low stress conditions heterogeneities may serve to concentrate stress and produce local cracking. However, since the volcanic source mechanics are previously

determined inputs in this model, viscoelastic effects on the rock anisotropy due to thermomechanical weakening will be confined to raypaths that pass nearby the magma source. Otherwise, assuming an elastic rheology is considered applicable to well-consolidated rocks when applied stresses, particularly deviatoric stresses, are small (below 10 to 30 MPa) [*Gurevich et al.*, 2011].

2. The sole cause of anisotropy in the rock is assumed to be stress-aligned microcracks, meaning an unstressed rock would be isotropic. This neglects other forms of anisotropy, such as bedding planes, fractures, and mineral fabric. However, the aim of this model is to investigate how volcanic stresses would affect shear wave splitting, so model-observation variations consistent with structural effects will still provide useful data.
3. Due to the use of the noninteractive approximation of *Sayers and Kachang* [1995], the cracks are assumed to be sufficiently sparse so that the overall rock compliance is simply a sum of the effects of individual cracks, disregarding any stress interaction between cracks. The analysis done by *Grechka and Kachang* [2006] shows that this is satisfactory for a range of irregular and intersecting approximately flat cracks up to substantial crack densities of at least $\epsilon = 0.15$.
4. The cracks are assumed to be dry, in the sense that there is no hydraulic interconnectivity between them. Changing the compliance ratio of the cracks would effectively simulate having water, oil, or any fluid other than air as crack fillers, but any interaction between the cracks must be excluded. This is a strong assumption to make in volcanic regions such as Asama, due to a prevalence of hydrothermal systems at volcanoes [*Aizawa et al.*, 2008] and a high water table in the Asama region [*Kazama and Okubo*, 2009]. This is perhaps the most significant of the assumptions, as microscale fluid flow between cracks is expected to modify the effect of small differential stress on overall anisotropy [*Zatsepin and Crampin*, 1997].
5. The exponential expression for specific crack area (s, see equation (5)) is simplified to a linear relationship [see *Gurevich et al.*, 2011]. This assumption has the effect of limiting the model accuracy to stresses that are small compared to the crack closing pressure. In our models, we approached this by setting maximum compressive stress to the crack closing pressure in the equations for calculating rock anisotropy for model blocks where the stress exceeds the closing pressure, in order to avoid a breakdown in the linear approximation.

2.4. Determining Shear Wave Splitting Parameters

In order to find the shear wave splitting parameters of a ray path, the incremental anisotropic effects on the seismogram for paths through each block that the ray travels through was calculated. Then the method of *Silver and Chan* [1991] was applied to calculate the splitting parameters from the predicted seismogram at the receiver. We adopted the method of calculating shear phase particle motions used by *Fischer et al.* [2000] and *Abt and Fischer* [2008]. For each ray segment, the Christoffel matrix was defined as *Babuška and Cara* [1991]:

$$m_{il} = \frac{1}{\rho}(c_{ijkl} n_j n_k) \tag{4}$$

where ρ is the density, and n_j and n_k are the ray path's directional cosines. The three eigenvalues of the Christoffel matrix are related to the anisotropic velocity and polarization properties of the wave. Given that $\lambda_1 > \lambda_2 > \lambda_3$, the fast shear wave component velocity, $V_f = (\lambda_2)^{\frac{1}{2}}$, and the slow component velocity, $V_s = (\lambda_3)^{\frac{1}{2}}$, with the corresponding eigenvectors giving the respective polarization directions. The time shift accrued for each ray segment, δt_n, is equal to $L(V_s^{-1} - V_f^{-1})$, where L is the segment length, and the fast direction, ϕ_n, is the fast polarization direction eigenvector orthogonal to the raypath. The resulting particle motion, u, for a path with m ray segments is defined by *Fischer et al.* [2000] as

$$u(\omega) = \left[\prod_{n=1}^{m} R^T(\phi_n) D(\delta t_n) R(\phi_n)\right] u_0(\omega) \tag{5}$$

where

$$R^T(\phi_n) = \begin{bmatrix} \cos\phi_n & \sin\phi_n \\ -\sin\phi_n & \cos\phi_n \end{bmatrix}$$

and

$$D(\delta tn) = \begin{bmatrix} e^{i\omega\delta t_n/2} & 0 \\ 0 & e^{-i\omega\delta t_n/2} \end{bmatrix}$$

The splitting parameters that best fit the ray path are those that, when applied to the split wave, return the most linear motion. This is achieved by finding the ϕ and δt values that produce the most singular covariance matrix (which is attained when the matrix has only one nonzero eigenvalue) [*Silver and Chan*, 1991].

The initial particle motion that propagated through the model, u_0, is a simple sine wavelet. The most common frequency window used for the crustal splitting analysis done at Asama by *Savage et al.* [2010] had a high pass of 3 Hz for local events (depth < 2.2 km below sea level) and around 1 Hz for regional events (depths between 40 and 156 km). We chose a wavelet with a frequency of 1 Hz to use in the model in order to represent a frequency found in the majority of frequency windows, while giving the wavelet an acceptable sample width (1000) for analysis.

Abt and Fischer [2008] performed a comparison between this particle perturbation method of calculating splitting parameters with calculations made using full synthetic waveforms generated using a pseudospectral approach. They considered a vertical boundary between two volumes with different anisotropic properties, finding that in the full-waveform case, interaction of the wave front with the boundary results in an observed difference in splitting measurements from the simple perturbation method, arising from waveform distortion and possible ray bending. These effects are most pronounced with large contrasts in effective velocity. This may present a problem for stress model examples where the size of a stress perturbation is comparable to the grid size, as large changes in stress orientation and, to a lesser degree, magnitude may be expected; however, since the modeled stress field expresses incremental spatial variations, these effects will diminish with higher block resolutions.

2.5. Volcanic Stress at Mount Asama

Mount Asama is an active andesitic volcano situated in central Japan at which numerous vulcanian eruptions occurred at the summit crater during the first half of the twentieth century (1910–1960), the frequency of which decreased after 1940. In the second half of the last century eruptions were more infrequent, culminating in a moderately large (volcanic explosivity index of 2) eruption in 2004 and minor eruptions in August 2008 and February 2009 [*Takeo et al.*, 2006; *Savage et al.*, 2010; *Murase et al.*, 2007; *Nagaoka et al.*, 2010]. The 2004 and subsequent eruptions have been well monitored and documented with both seismic and geodetic data, allowing the various magmatic sources to be determined [*Takagi et al.*, 2005; *Takeo et al.*, 2006]. This forms the basis for a first-order constraint on the volcanic stress to be used in the forward model.

In order to model the contribution to the stress field from processes associated with volcanism for input into the forward model, a priori knowledge of the magma plumbing system is required. The 2004 eruption at Mount Asama was accompanied by surface deformation and seismicity that has been used to infer a likely magma supply path beneath Asama [*Takagi et al.*, 2005; *Takeo et al.*, 2006]. Using geodetic and seismic data, *Takeo et al.* [2006] proposed that between June 2004 and March 2005, 6.8×10^6 m^3 of magma was intruded into a near-vertical dyke system trending broadly E-W and extending from 3 km to 5.1 km below sea level. This dyke model has subsequently been imaged as part of a zone of high seismic velocity that signifies repeated past dyke intrusion and cooling [*Aoki et al.*, 2009]. In the final models used in the anisotropy modeling we use the dyke inflation parameters found by *Takeo et al.* [2006] and later corroborated by *Aoki et al.* [2013]. It is worth noting that *Takagi et al.* [2005] and *Takeo et al.* [2006] both include two small magma reservoirs along the magma ascent path; however, we found that their stress contribution had little effect on the regional stress conditions with respect to the dyke stress contribution. Noninclusion of these reservoirs, located at 1.5 and 2.2 km below sea level [*Takagi et al.*, 2005], means that raypaths traveling close to the caldera of Asama may be poorly modeled.

2.6. Regional Stress

Any consideration of stress-induced anisotropy would be incomplete without the inclusion of the effects of the regional stress field. In this paper, the regional stress field will refer to the combined effects of confining pressure and tectonic forces. We assume the regional stress to be constant through time, in contrast to the stress field exerted by the volcano. Interaction between regional stress and local stresses from magma emplacement is a central theme in interpreting seismic anisotropy changes during volcanic eruptions [e.g., *Gerst and Savage*, 2004; *Johnson et al.*, 2011]. *Roman and Heron* [2007] studied the link between the distribution of volcano-tectonic earthquakes (VT) and Coulomb stress modeling of dyke inflation, finding that VT

Table 2. Elastic Properties for Rocks With Dry and Wet-Filled Cracks Given by *Crampin* [1985][a]

Dry Cracks		
$c_{1111} = 51.546$	$c_{2222} = 83.477$	$c_{3333} = 83.477$
$c_{1122} = 17.175$	$c_{2233} = 25.155$	$c_{3311} = 17.175$
$c_{1212} = 23.240$	$c_{2323} = 29.161$	$c_{3131} = 23.240$
Saturated Cracks		
$c_{1111} = 87.464$	$c_{2222} = 87.464$	$c_{3333} = 87.464$
$c_{1122} = 29.142$	$c_{2233} = 29.142$	$c_{3311} = 29.142$
$c_{1212} = 23.240$	$c_{2323} = 29.161$	$c_{3131} = 23.240$

[a]Values are shown in GPa.

seismicity patterns are controlled by the regional stress regime and strength. They show that VT seismicity models for a dyke being emplaced in weakly and strongly deviatoric regional stress conditions fit well with VT data for eruptions at Mount Usu and Miyake-jima volcanoes (both situated in Japan), respectively, as suited by their tectonic setting.

Confining pressures increase with depth due to lithostatic overburden [*Turcotte and Schubert*, 2002]. Increasing isotropic pressure will influence microcracks equally regardless of the orientation and thus would not be expected to affect the overall rock anisotropy. This notion is consistent with the analytical stress-anisotropy relationship used in this paper. However, increased crack closure at higher lithostatic pressures means that intrinsic lattice preferred orientations (LPO) will begin to dominate the elastic properties of the rock mass [*Ji et al.*, 2013]. At the point at which microcracks and other discontinuities have been closed, seismic anisotropy must be assumed to arise from a rock's LPO. In essence, due to the relationship between depth and lithostatic pressure mentioned above, this means that a maximum depth, below which anisotropy cannot be attributed to the current state of stress, can be estimated. Assuming a crustal density of 2900 kg m^{-3} gives a depth of 1.75 km for crack closing pressures of 50 MPa [*Gurevich et al.*, 2011] and 3.5–7.0 km for crack closing pressures of 100–200 MPa [*Christensen*, 1996]. Pressure gradients can be up to 2 times steeper in regions influenced by horizontal tectonic stresses in the upper lithosphere, or by flexurally induced vertical loading in the lower lithosphere, resulting in a smaller maximum depth at which these pressures are reached [*Petrini and Podladchikov*, 2000]. The presence of an incompressible or near-incompressible fluid (such as water) that is confined to the microcracks would significantly increase the pressures at which the cracks would stay open [*Zatsepin and Crampin*, 1997].

In addition to confining pressure from rock overburden, there will be a component of differential stress exerted by tectonic forces. Folding and thrust belts demonstrate the historic presence of a differential stress field, and the occurrence of earthquakes is evidence of the ongoing existence of differential stresses, the configuration of which determines the mode of failure and faulting in geologic materials [*Anderson*, 1951]. Following the "Wallace-Bolt" hypothesis (i.e., fault slip occurs in the direction of maximum resolved shear traction, [*McKenzie*, 1969]), the orientation of the principal stress axes can be retrieved from the earthquake fault plane solutions. *Townend and Zoback* [2006] calculated principal stress orientations and a measure of their relative magnitudes in central Japan by inverting focal mechanisms for earthquake clusters (see Figure 2).

Relative principal stress magnitudes were expressed as ϕ, such that

$$\phi = \frac{\sigma_2 - \sigma_3}{\sigma_1 - \sigma_3} \tag{6}$$

where σ_1, σ_2, and σ_3 are the three principal stresses. Values of ϕ approaching zero are indicative of stress conditions, where $\sigma_2 = \sigma_3$ and $\sigma_1 \gg \sigma_2, \sigma_3$. As stress becomes isotropic, ϕ will reach unity.

The nearest maximum horizontal stress directions (σ_{Hmax}) calculated near Asama lie to the west of the caldera. Directions lie roughly parallel to the strike of the dyke (N64°W) between N58°W and N84°W. Values for σ_{Hmax} calculated from deeper clusters of earthquakes (8 km), which are all situated northwest of the caldera, trend slightly more east-west than the σ_{Hmax} value calculated from shallower earthquakes, which trends more northwest-southeast. The stress regime in the area is mainly strike-slip, with one measurement exhibiting a reverse stress regime. According to the Andersonian theory of faulting, having strike-slip and reverse stress regimes in proximity could be an indication of σ_2 and σ_3 being roughly equivalent, since the transition between the regimes represents an inversion between the two. The closest measurement to Asama has a ϕ of 0.0779 [*Townend and Zoback*, 2006], which reinforces this hypothesis. The mean value of ϕ for measurements by Townend and Zoback in the region shown in Figure 2 is ~0.25.

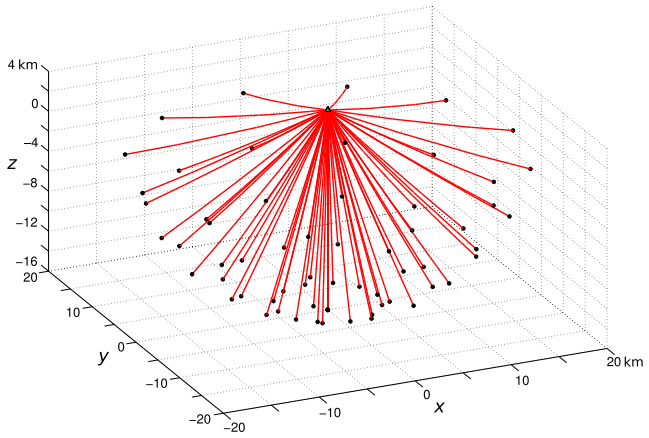

Figure 3. Ray path configuration used in the test cases. All ray paths have a length of 20 km and are positioned to have straight-line surface incidence angles at 15° intervals from 0° to 75° at back azimuths in 30° intervals. The surface of the model is at 4 km.

3. Results

3.1. Anisotropy Model Testing

We tested the forward model by using effective elastic constants for both dry and fluid-filled cracked media given by *Crampin* [1985] (shown in Table 2) as a benchmark. To do this, an arbitrary ray path configuration with a range of event-station azimuths and incidence angles was created (see Figure 3).

In each case, there is a set of cracks dipping vertically, striking east-west. The forward model was configured to assign the same elastic constants to every model block. As can be seen in Figure 4, the forward model was able to faithfully recreate the results that Crampin made in 1985. Similar tests were done with the stiffness matrix rotated in order to represent cracks with planes parallel to the horizontal. They display a tangential arrangement of polarizations with delay times increasing with larger incidence angles for dry cracks and a more complex pattern for saturated cracks showing a polarization flip between radial directions at low incidence angles and tangential directions for rays that are more steeply inclined to the plane of the cracks.

In order to produce a comparable forward model using the stress-induced anisotropy calculations, a 50 km by 50 km by 34 km model space was created with a uniaxial stress of 12.5 MPa oriented east-west. As before, a range of equidistant event/station pairs were used in order to observe the splitting effects in a range of azimuths and incidence angles. As can be seen in Figure 5, the results are the same morphologically as the dry cracks shown in Figure 4, except that fast directions are rotated toward the tangential near the North and South Poles. As the derivation of the stiffness matrix for Figure 5 is based on the assumption that the

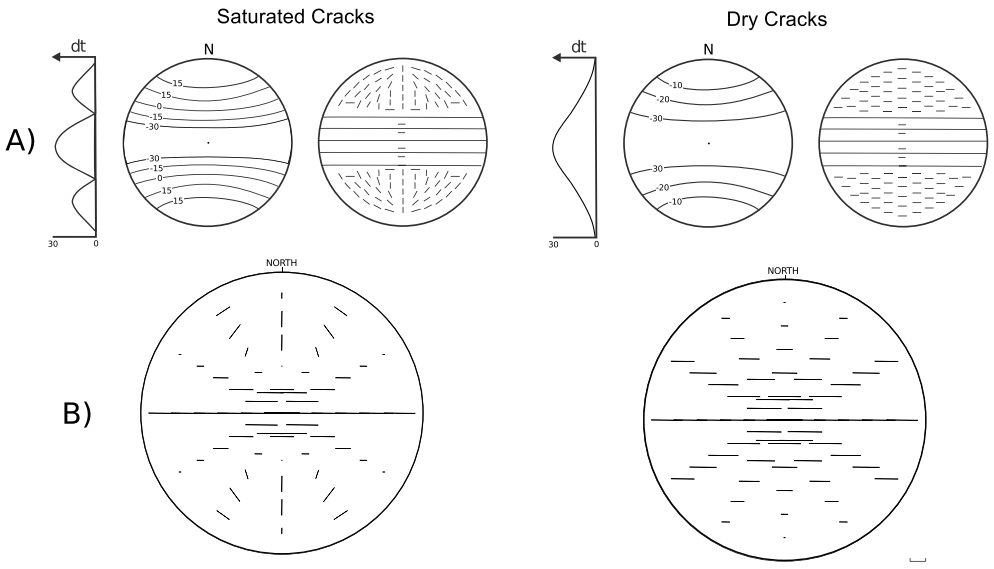

Figure 4. Equal-area stereographs showing shear wave polarizations and delay times for dry cracks and cracks saturated with a liquid. (a) Original results from *Crampin* [1985], with (left) delay time contours with a north-south section plotted and (right) horizontal polarizations plotted as solid lines. (b) Results from the model using the same elastic configuration. Fast shear wave polarizations are plotted, with the size of each line representing the relative delay time.

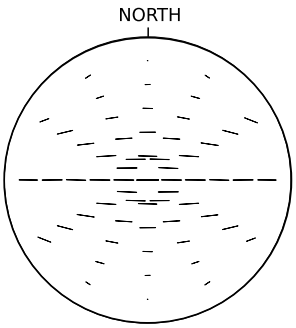

Figure 5. Equal-area stereograph showing model results for a model that has had 1 cm of shortening applied in the east-west direction. The parameters used in calculating the elastic properties of the subsurface were $Z_{to} = 0.024\,\text{GPa}^{-1}$, $B = 1.76$, crack closing pressure $P_c = 19.2\,\text{MPa}$, $\mu = 20\,\text{GPa}$, and $K = 50\,\text{GPa}$.

cracks are dry and noninteractive, we expect the observed similarities in comparative delay times and fast directions for this raypath configuration.

3.2. Stress Model Analysis

In order to investigate any relationship between ray path, dyke stress, and shear wave splitting, we calculated stress models derived from the known dyke and material properties at Mount Asama and compared the dyke stress along various event raypaths to the respective shear wave splitting measurements. Dyke stresses were considered independently of gravitational and tectonic forces, since in this case we are exclusively assessing the relative change of stress rather than the absolute degree of shear wave splitting along a ray path. This type of analysis can be done on events occurring deeper than the base of the model without the need for assumptions to be made about shear wave splitting accrued before the ray's entrance into the model space. Data from *Savage et al.* [2010] were analyzed in this way. Here we show results from 32 regional events measured at station AVO between January 2004 and December 2005 and 35 local events that occurred between June 2004 and February 2005. In particular, we discuss results from AVO due to the original study observing a high degree of correlation between splitting measurements made there over time and ground deformation over the period spanning the eruption.

Stresses for a dyke opening model alone were unrealistically large, as high as 100 MPa at the dyke edges. Such high stresses are an artifact of the application of a uniform opening on the dyke plane in the model. Figure 6 shows the extent of the stress magnitudes, which decrease quickly with distance from the dyke face to roughly 10 MPa at less than 1 km from the dyke. Elastic parameters for the model were determined from the seismic velocity model of *Aoki et al.* [2009]. Results for regional events recorded at AVO and local events show no correlation between the dyke stress felt along the raypath and delay time. At station AVO, the strongest dyke stress conditions for the majority of the raypaths were felt at the depth of the dyke, between 3 and 5 km deep. Results for regional events arriving at AVO (see Figure 6) experience maximum compressive dyke stresses of 1.0–1.1 MPa, and local raypaths (see Figure 7) experience similar maximum compressive dyke stresses of 0.9–1.1 MPa.

Dyke stresses were added to regional stress backgrounds during the stress model regridding process. In each case, the regional stress followed a one-dimensional relationship with depth. Isotropic stress increases with depth (where we assumed a constant density of $3000\,\text{kg m}^{-3}$ in the relationship), as does deviatoric stresses with σ_1 and σ_3 being 2.5%, 5%, and 10% higher and lower, respectively, than σ_2. In each case, σ_2 was

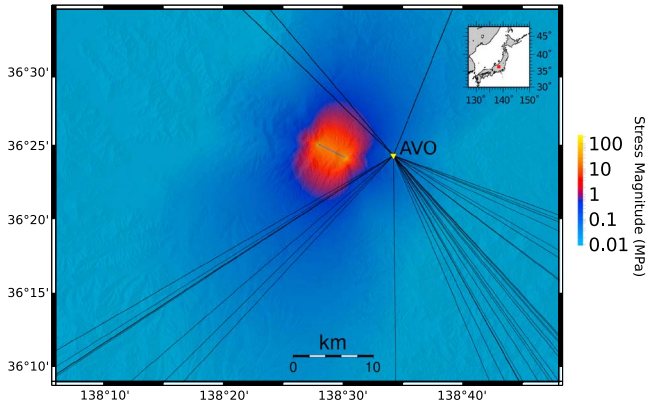

Figure 6. Stress model results showing maximum stress magnitudes created by the dyke associated with the 2004 eruption of Mount Asama, Japan, in a horizontal cross section 1 km below sea level. Also shown are incoming rays at station AVO for events occurring in 2004. Earthquake depths range from 61 to 366 km.

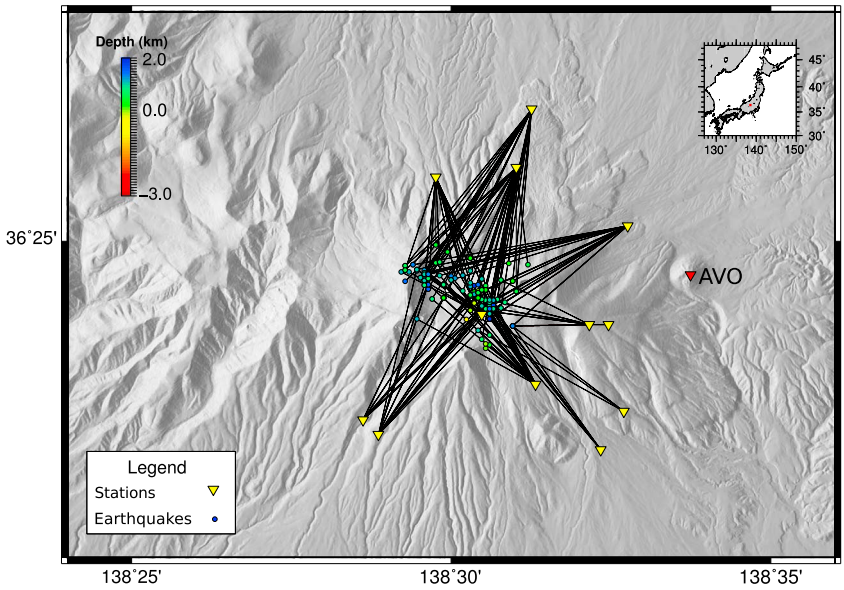

Figure 7. Local data set for shallow earthquakes at Mount Asama. All earthquakes occurred between 1 May 2004 and 1 February 2005.

set by the same ρgh relationship as in the isotropic case. Figure 8 shows results indicating the ratio between magnitude of the deviatoric stress and the overall stress ($\Delta\sigma/P$). Generally, this was small at all depths apart from cells in close proximity to the dyke edges. For larger deviatoric stresses (20%), $\Delta\sigma/P$ near the dyke face is actually lower than in the surrounding region, as the outward pressure directly counteracts the regional stress (see Figure 8c).

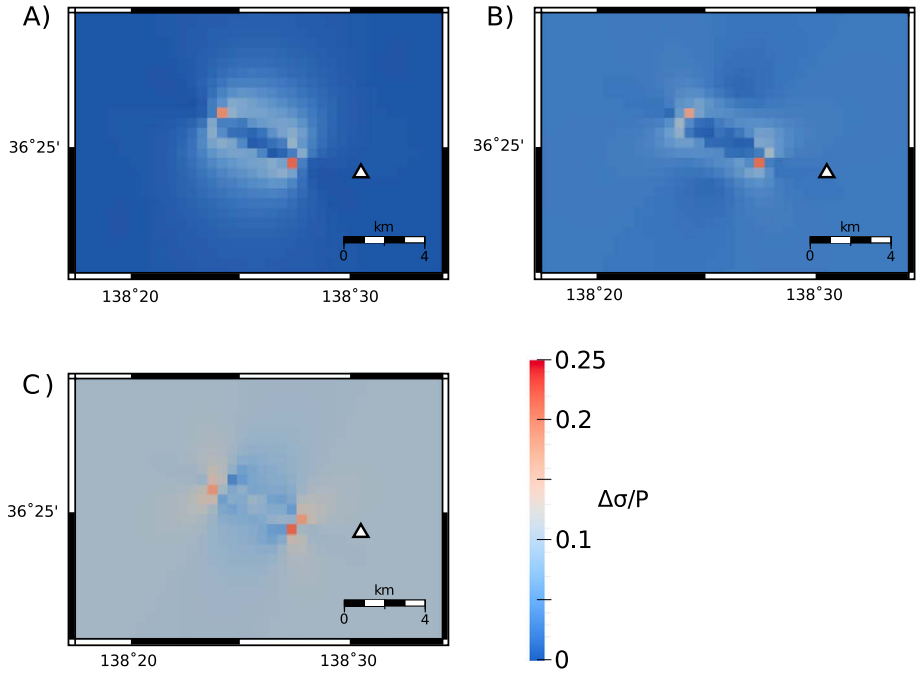

Figure 8. Stress model results showing the ratio between deviatoric stress magnitude ($\Delta\sigma$) and pressure (P) 1 km below sea level. The deviatoric stress magnitude is calculated as the difference between the maximum compressive stress magnitude and the average principal stress magnitude. (a) Effect of dyke expansion in a lithostatic stress regime, (b) a strike-slip stress regime where σ_1 is 5% greater than σ_3, and (c) a strike-slip regime where σ_1 is 10% greater than σ_3.

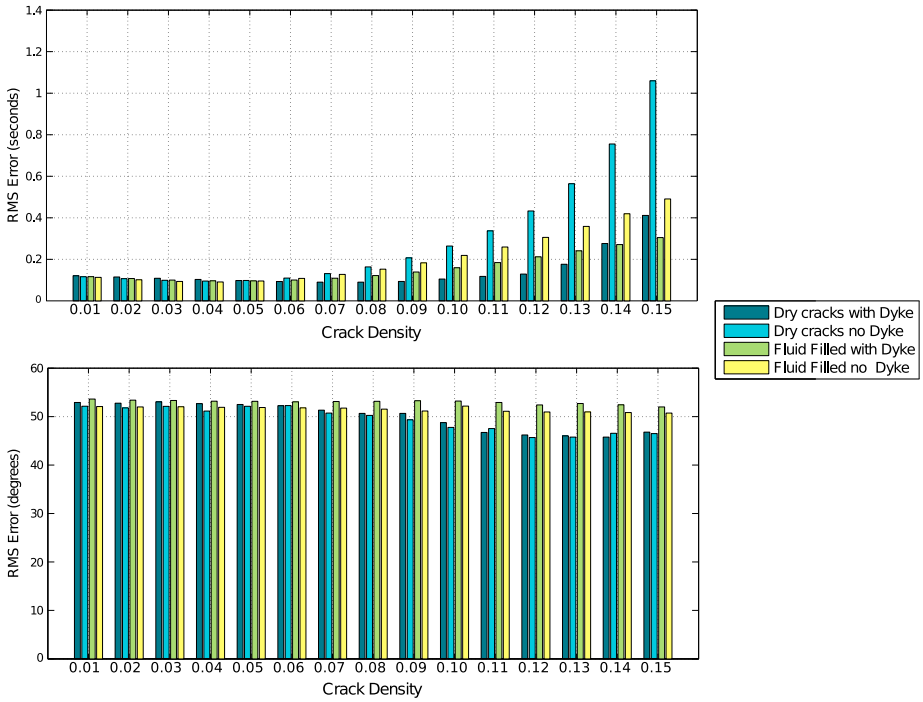

Figure 9. Chart showing root mean square errors between modeled and real shear wave splitting measurements from local events at Mount Asama, comparing solutions at different crack densities (ϵ) for Hudson's fluid-filled and dry crack calculations. The stress models used have increasing pressure with depth, according to ρgz, with a regional stress with a differential value of 5% of the background pressure.

3.3. Elastic Tensor

The elastic tensor of each block is the governing parameter for seismic velocity and therefore central to the results taken from this modeling. Taking the calculations from *Hudson* [1981] for both dry and fluid-filled cracks, synthetic splitting measurements were calculated for a range of crack densities and stress models. For the stress model, dyke stresses were added to regional stress backgrounds during the stress model regridding process, as discussed in section 3.2.

We tested the effects of using various forward models incorporating Hudson's elastic parameters on the data set of 35 local events, comprising 86 individual station-event pairs (see Figure 7). Results for both dry and fluid-filled crack models show that synthetic fast directions were poorly aligned with measurements regardless of ϵ, with a mean model-measurement misfit of 45–55° (see Figure 9). Increasing crack density made little impact on fast direction, as the orientation of anisotropy is consistent while using the same stress model. *Savage et al.* [2010] found misfits of 38–52° in a simple comparison between the measurements and stress directions found from Coulomb stress modeling of the dyke, as well as the two inflating magma chambers of *Takagi et al.* [2005]. Here delay times were best modeled with ϵ values of 0.04–0.08, depending on the stress model used and whether dry or fluid-filled crack equations were employed. For the best fitting models the root mean square error of delay times was around 0.1 s, similar to the mean measured delay time for the events (see Figure 9). As this approach assumes a constant crack density throughout the model, we found that there was a broad correlation between length of raypath and modeled delay times. Such a correlation, however, is not present in the measured data.

Comparisons between different models were made by calculating the mean difference between two sets of results, such as

$$\text{Mean difference} = \frac{\sum_{i=1}^{N} |x_i^1 - x_i^2|}{N} \tag{7}$$

where i is each individual measurement. Mean angular differences in fast direction between models having a regional stress where σ_1 was 5% larger than σ_3 (the smallest modeled) with and without the dyke added

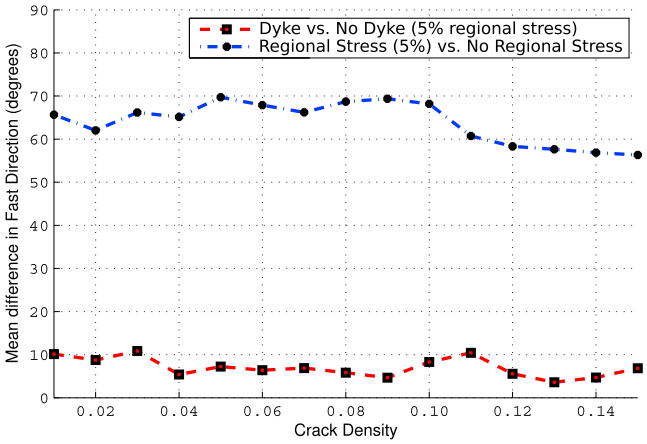

Figure 10. A comparison of mean differences between modeled results. Red squares represent two models with a 5% differential regional stress with and without an inflating dyke, and blue circles represent two models with an inflating dyke with and without the background stress. Results show that the presence of the differential regional stress is much more influential on fast directions than the dyke.

were between 5 and 10°, depending on the crack density used. In comparison, mean differences between two models both containing a dyke, with one having the differential regional stress as before and one without were 58–70° (see Figure 10). This indicates that for these events, the inclusion of the differential regional stresses used is more significant than the dyke itself. For the larger differential regional stress used, at 20%, mean differences between models with and without a dyke were <5°.

We also tested models using the analytical relationship between stress and anisotropy discussed in section 2.5, taking into account stress orientation and magnitude. Modeled delay times were invariably significantly smaller than those measured (see Figure 11). This was due to a combination of short path lengths through a weakly anisotropic medium as well as stresses exceeding the theoretical crack closure pressure at relatively shallow depths. In the case of a nonisotropic background stress, modeled fast directions were dominated by the regional stress direction. Figures 12a and 12b show comparisons between models with and without dykes. Generally, differences between models were negligible for all regional stress considerations that were modeled. Results are quantized to intervals of 0.001 s due to that being the sampling

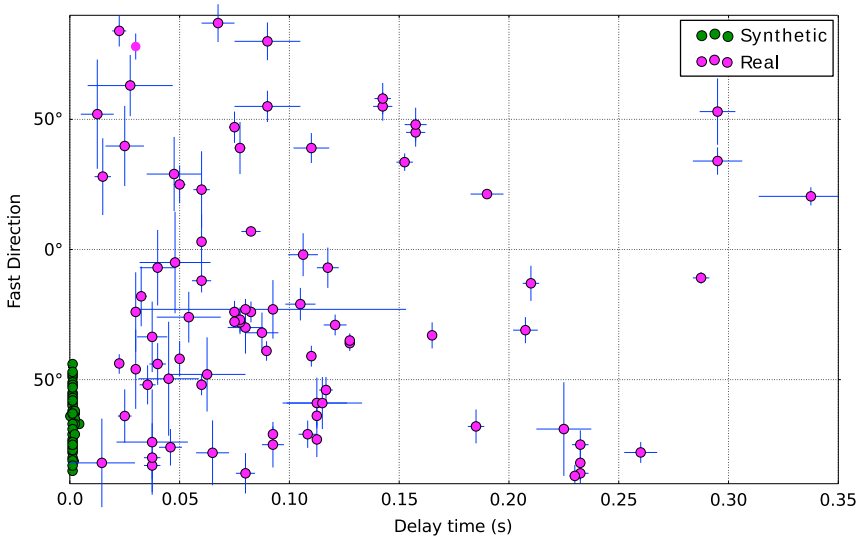

Figure 11. Measured and modeled results from local earthquakes at Mount Asama that occurred around the 2004 eruption. Synthetic results, taken from a model with a tangential crack compliance value of 0.024 GPa^{-1} and a Z_{T0}/Z_{N0} ratio of 1.76 in a model with a dyke situated within a regional stress field where σ_1 is 5% greater than σ_3, were distributed near the regional stress direction (W70N) and had significantly smaller delay times than those measured.

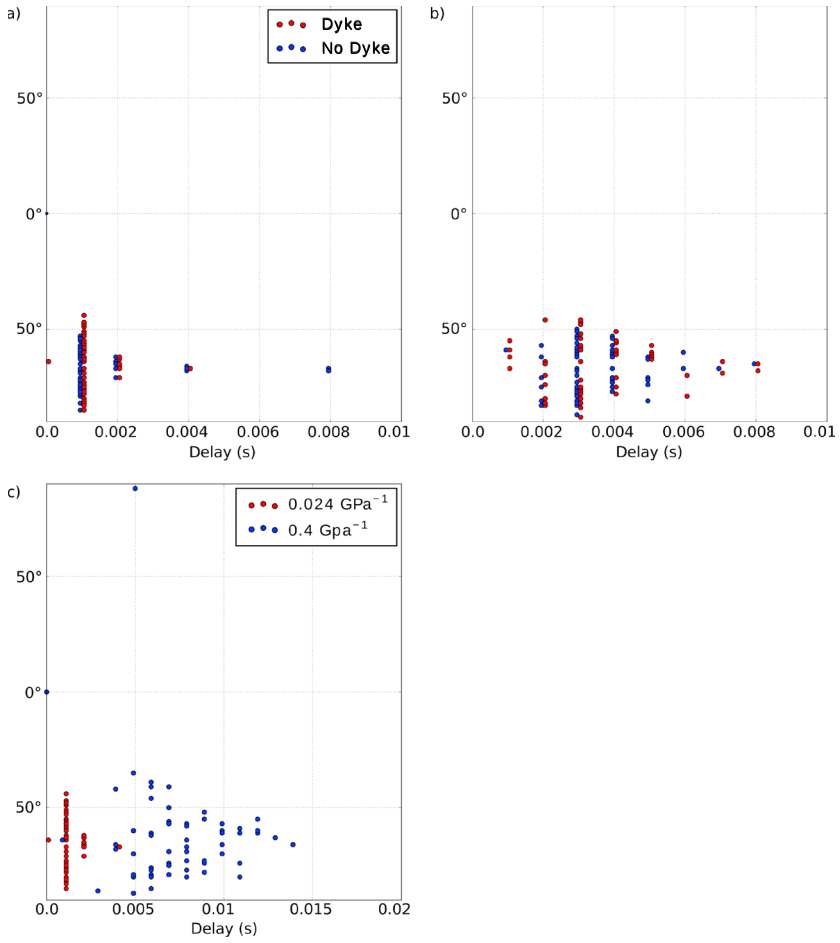

Figure 12. Model result comparisons. (a and b) Comparisons of synthetic measurements between models with and without a dyke for regional stress fields where σ_1 is 5% and 20% greater than σ_3, respectively. Tangential crack compliance in both plots is 0.024 GPa^{-1}. (c) Effect of increasing tangential crack compliance from 0.024 GPa^{-1} to 0.4 GPa^{-1}. Results are slightly offset for visual clarity. In each plot, data sets are offset by 0.1 ms for clarity.

frequency of the synthetic wave. The measured average of the data set was 0.10 s, and we consider delays to be significant only if they exceed 0.01 s, which is 1 order of magnitude greater than the model sampling frequency of 0.001 s, as well as being double the average standard error for the original. Figure 12c shows the model sensitivity to crack compliance; in all results shown in Figure 12, a normal-to-tangential crack compliance ratio of 1.76 was used and increasing tangential crack compliance results in greater modeled delay times.

The model was unable to account for the degree of anisotropy measured by stations at Asama. Local raypaths are of lengths between 0.6 and 5.2 km, with measured anisotropy values up to 0.4 s, averaging 0.11 s. The same raypaths gave an average of 0.0012 s in models with a tangential crack compliance of 0.024 GPa^{-1} (Figure 11). The average strength of anisotropy given by *Savage et al.* [2010], calculated as the fractional velocity ratio $((v_1 - v_2)/v_1$, v_1, and v_2 being the fast and slow shear wave velocities, respectively), is 6%. Making the cracks significantly less stiff than those modeled by *Gurevich et al.* [2011] in order to test model sensitivity (using a tangential compliance value of 0.4 GPa^{-1}) results in an increase in delay times; however, no delays exceeded 0.015 s. With the analytic solution for anisotropy used here, we find that highly deviatoric stress conditions are needed to produce such significant anisotropy. Using the test model parameters used to find the results of Figure 5 (tangential crack compliance of 0.024 GPa^{-1} and a compliance ratio of 1.76), the maximum velocity ratio for a uniaxial stress of 12.5 MPa was 3.1%, with nonuniaxial stresses being significantly lower.

4. Discussion

Using Hudson's calculations to derive elastic tensors gave the best fitting results at crack densities very similar to that found by *Savage et al.* [2010] from local earthquakes (4.4×10^{-2}). Errors between the model and measurements were relatively large; however, the mean delay times were similar for models at the above crack density. We observe that the modeled fast direction RMS misfits are in the region of 10° larger than misfits found by the original study using comparisons between Coulomb modeling and fast directions. The same forward models also displayed more sensitivity to regional stresses than to inclusion of the dyke itself. This suggests that accurately defining the background stress conditions is an important step to a more comprehensive understanding of the interaction between volcanic stresses and anisotropy.

In models using the full analytic solution for dry crack anisotropy, modeled delay times were extremely low in comparison to measurements. Using a dry crack model such as this will necessarily underestimate the degree of anisotropy because lower stress conditions are needed to close an air-filled void than to close voids saturated with fluids which are near incompressible (i.e., water). This is due to *Sayers and Kachang*'s [1995] original formulae for brittle rock anisotropy making an approximation that assumes a high normal crack compliance. If the cracks are filled with a fluid and there is microscale fluid flow between them, this could have strong implications for modeling stress-induced anisotropy. Wave-induced flow between cracks will affect dispersion and attenuation [*Chapman et al.*, 2002; *Gurevich et al.*, 2010], as well as anisotropy [*Collet and Gurevich*, 2013]. On a longer time scale, this fluid flow may create conditions in which relatively small levels of differential stress can produce significant changes in anisotropy. This was concluded by *Zatsepin and Crampin* [1997], who posit that hydraulically isolated sets of fluid-filled cracks may exist to depths of many kilometers. Our models show that variations in anisotropy around volcanoes as dyke stresses quickly become small compared to expected lithostatic pressure, with or without a regional stress (see Figure 7). Thus, if stress-induced anisotropy caused the measured changes at Asama [*Savage et al.*, 2010], then hydraulic interaction between cracks is likely to have occurred. A small differential stress, when applied to such a system, will produce a pressure gradient along which fluid migration can occur from cracks oriented perpendicularly to maximum compressive stress to those aligned otherwise. This results in excess pore fluid pressure within the crack that is dependent on differential stress and the relative orientation of the crack [*Zatsepin and Crampin*, 1997]. If the fluid is near incompressible, the total crack volume in the medium will not be significantly changed. Fluid under pressure entrained in cracks at depth will also prevent their closure despite increasing lithostatic pressure, provided no upward macroscale fluid diffusion can occur.

The above consideration is approximated by the approach using Hudson's formulations for fluid-filled cracks, as strength of anisotropy does not depend on differential stress magnitudes. However, it is unlikely that the strength of anisotropy is constant and, as evidenced by the unsatisfactory model fit, that it is entirely controlled by principal stress orientation. Strength of anisotropy may be strongly affected by the lithology and formation and deformation history of the rock, as well as other features such as other stress sources, fractures, mineral fabrics, and rock unit interfaces.

4.1. Considerations for Future Work

A logical development to this method is to use measurements made outside a volcano's active period to invert for anisotropic structure (using methods such as that of *Abt and Fischer* [2008] or *Wookey* [2012] and then applying a model such as *Hudson*'s [1981] or the APE model of *Zatsepin and Crampin* [1997] to find properties of the rock mass (e.g., crack density) from that. Providing a "background" model of anisotropy in this way could be key to setting a benchmark from which subsequent measurements can be compared. This would potentially not only provide more robustness in using shear wave splitting as an eruption-forecasting tool but also help to elucidate the source of temporally changing anisotropy as changes would be relative to what we already believe to be present. This is most important when attempting to interpret changes in measured anisotropy, especially when trying to forecast volcanic activity as data may be sparse.

As volcanic eruptions are often accompanied by changes to the spatial distribution and intensity of the volcanic hydrothermal system, changing fluid properties (both physical and chemical) could be a mechanism for dynamic anisotropy conditions associated with volcanic activity. Fluid flow and gas emission are very much affected by thermal conditions and subsurface permeability, in addition to changing stress properties. Studies on the stress-dependent compliance properties of volcanic rocks would be useful to investigate these effects. Detecting such changes can feasibly be done with seismic methods; V_P/V_s can be a proxy for fluid or gas saturation [*Wang et al.*, 2012]. *Johnson and Poland* [2013] identified changes in shear wave

splitting measurements and V_p/V_s at Mount Kīlauea associated with degassing of SO_2 rather than changes in stress. *Angerer et al.* [2002], using the anisotropic poro-elastic (APE) model of *Zatsepin and Crampin* [1997], studied the effect of changing fluid pressure on crack content, seismic velocity, and anisotropy of a dolomite reservoir, finding *S* wave anisotropy changes of 5.8% after injection of high-pressure CO_2, as well as a 90° flip in fast polarization to become stress-perpendicular.

Changes in anisotropy not due to stress changes should also be addressed. Dynamic changes of material filling cracks, and therefore their elastic properties, were not modeled here, although they may have a substantial effect on resultant anisotropy through the influences explained above. The aforementioned analytical solution only considers the bulk and shear moduli of the intact, isotropic rock. Naturally, the effective bulk and shear moduli of the resulting anisotropic material are changed depending on the distribution of open cracks. The solution for the anisotropic term in the stiffness tensor is factored by radial and tangential crack compliances; however, the ratio between these compliances is poorly defined. *Gurevich et al.* [2011] give the ratio $B_N/B_T = 1.76$ as found from fitting the rock physics model outlined in *Angus et al.* [2009] to results from tests made on a sample of Barre Granite. The same study by *Angus et al.* [2009] applied their fitting method to data on sedimentary rocks, finding that compliance ratios range between 0.0 and 2.0 and cluster around 0.6. In addition to microscale fluid flow, the contents of the microcracks are expected to alter B_N/B_T, as the change in compressibility of the fluid or gas in the crack will have a disproportionate effect of the normal compliance over the tangential compliance. *Sayers and Han* [2002] and especially *Angus et al.* [2012], while studying sedimentary rocks, find that ratios in dry samples and saturated samples are indeed different. *Angus et al.* [2012] showed that crack saturation had the effect of tightly clustering ratios around 0.5, in comparison to dry samples that showed ratios distributed between 0.4 and 2.0. There is also the issue of the crack compliance value itself, which can significantly affect model results (see Figure 12). These complications present a challenge when attempting to model complex anisotropic systems.

Finally, we have modeled the dyke emplacement using an elastic finite element method, which offers better control over the model space (i.e., the geometry of the dyke interface and surface topography) than Coulomb stress modeling. As already mentioned, viscoelastic deformation near the magma pathway would likely increase the needed pressure to produce the observed surface deformation. The converse of this is that viscoelastic deformation in an aureole around the dyke will act to reduce the magnitude of the static stress field. Currently it is difficult to quantify the combined effect on anisotropy of both stress and viscoelastic deformation. Furthermore, during the dyke emplacement process the stress state will evolve in a different way to modeling whole-dyke inflation, as has been done in our method. As a dyke is emplaced, magma overpressure is greatest at the edge that is propagating through country rock, producing large, localized stress magnitudes [*Taisne et al.*, 2011], which may significantly alter the stress profile of the region.

5. Conclusion

We have developed a method for three-dimensional modeling of shear wave splitting in the crust and applied this model to the 2004 eruption at Mount Asama, Japan, in order to investigate the link between the crack closure model of stress-induced anisotropy and observed measurements. Results showed that dyke stresses are small relative to overall stress conditions expected from the rock overburden at depth. We found that applying both a simplistic measure of crack anisotropy and an analytic dry crack anisotropy relationship that takes into account the stress state produced variations in both strength and orientation of anisotropy smaller than those observed during the eruption. We also observe that for the dyke to have a significant effect on the anisotropy, the deviatoric regional stress must be small with the magnitude of σ_1 being less than 5% greater than σ_3. However, the dynamic rupture process of the dyke during its ascent will concentrate stress at the edge of propagation due to magma accumulation, meaning that we may be underestimating dyke stresses during emplacement. From these findings we conclude that dry crack closure due to dyke-induced stress changes is not a candidate for changing anisotropy conditions. This would suggest a number of possible alternatives, given that the possibility that changes in splitting measurements represent spatial heterogeneity in anisotropy was addressed by *Savage et al.* [2010]. The process for creating anisotropy may be different from the one used in the model; for example, the APE model of *Zatsepin and Crampin* [1997], where very small changes in the deviatoric stress component can produce relatively large changes in crack anisotropy, could be applicable. Alternatively, there may be a process associated with the volcanism that changes the crack properties themselves, in terms of either their distribution or overall contribution to anisotropy such as changing properties in fluid or gas pressure and saturation.

How stress-induced anisotropy is determined for in situ rocks is important considering that the response of anisotropy to stress is dependent on lithology, crack density, and fluid saturation. As the crust is heterogeneous at scales down to a meter or less, building a complete model of how anisotropy is sampled by shear waves is a difficult task. In modeling a dynamic system, however, we can investigate singular processes that changing anisotropic conditions may be attributed to. We suggest this approach should be developed to produce an anisotropic benchmark, with the use of a data inversion technique, on top of which measured changes can be compared and their source better constrained.

Appendix A: Writing the C_{ijkl} Tensor in the Second Order

The C_{ijkl}, or elastic, tensor defines the general form of Hooke's law relating stress to strain, i.e.,

$$\sigma_{ij} = C_{ijkl}\epsilon_{kl}$$

The symmetries of both the stress and strain tensor allow the i and j, and the k and l indices to be freely swapped. Furthermore, the two index pairs (i, j) and (k, l) can be swapped due to the existence of a quadratic strain energy density function [*Babuška and Cara*, 1991]. Thus, the number of independent elastic coefficients for an anisotropic medium can be reduced to 21 and denoted with the use of a 6×6 matrix, C_{ij}. The relation between C_{ij} and c_{ijkl} is as follows:

$$C_{ij} = \begin{bmatrix} c_{1111} & c_{1122} & c_{1133} & c_{1123} & c_{1113} & c_{1112} \\ c_{2211} & c_{2222} & c_{2233} & c_{2223} & c_{2213} & c_{2212} \\ c_{3311} & c_{3322} & c_{3333} & c_{3323} & c_{3313} & c_{3312} \\ c_{2311} & c_{2322} & c_{2333} & c_{2323} & c_{2313} & c_{2312} \\ c_{1311} & c_{1322} & c_{1333} & c_{1323} & c_{1313} & c_{1312} \\ c_{1211} & c_{1222} & c_{1233} & c_{1223} & c_{1213} & c_{1212} \end{bmatrix}$$

For a more in depth discussion, see *Babuška and Cara* [1991].

Acknowledgments

We thank our two reviewers, Nico Fournier and Benoit Taisne, for their invaluable commentary on this paper. We would like to thank the Marsden Foundation, ERI, and Victoria University of Wellington for funding contributions. We would also like to acknowledge ERI and GNS for data and accommodation. We also thank Sapi Karalliyadda and Katrina Jacobs for their helpful discussions and Olivia Collett and John Townend for their indispensable contributions. Splitting data used in the analysis were taken from *Savage et al.* [2010] and can be obtained from Martha Savage via direct contact (martha.savage@vuw.ac.nz). Geodetic data used in the stress model were taken from *Takeo et al.* [2006] and can be obtained from Yosuke Aoki via direct contact (yaoki.eri.u-tokyo.ac.jp).

References

Aagaard, B., S. Kientz, M. Knepley, L. Strand, and C. Williams (2007), Pylith user manual version 1.0. [Available at www.geodynamics.org.]

Aagaard, B. T., M. G. Knepley, and C. A. Williams (2013), A domain decomposition approach to implementing fault slip in finite-element models of quasi-static and dynamic crustal deformation, *J. Geophys. Res. Solid Earth*, *118*, 3059–3079, doi:10.1002/jgrb.50217.

Abt, D. L., and K. M. Fischer (2008), Resolving three-dimensional anisotropic structure with shear wave splitting tomography, *Geophys. J. Int.*, *173*(3), 859–886.

Aizawa, K., Y. Ogawa, T. Hashimoto, T. Koyama, W. Kanda, Y. Yamaya, M. Mishina, and T. Kagiyama (2008), Shallow resistivity structure of Asama Volcano and its implications for magma ascent process in the 2004 eruption, *J. Volcanol. Geotherm. Res.*, *173*(3), 165–177.

Anderson, E. M. (1951), *The Dynamics of Faulting*, 2nd ed., 206 pp., Oliver and Boyd, Edinburgh, U. K.

Angerer, E., S. Crampin, X.-Y. Li, and T. L. Davis (2002), Processing, modelling and predicting time-lapse effects of overpressured fluid-injection in a fractured reservoir, *Geophys. J. Int.*, *149*(2), 267–280.

Angus, D. A., J. P. Verdon, Q. J. Fisher, and J.-M. Kendall (2009), Exploring trends in microcrack properties of sedimentary rocks: An audit of dry-core velocity-stress measurements, *Geophysics*, *74*(5), E193–E203.

Angus, D. A., Q. J. Fisher, and J. P. Verdon (2012), Exploring trends in microcrack properties of sedimentary rocks: An audit of dry and water saturated sandstone core velocity–stress measurements, *Int. J. Geosci.*, *3*, 822–833.

Aoki, Y., et al. (2009), *P*-wave velocity structure beneath Asama Volcano, Japan, inferred from active source seismic experiment, *J. Volcanol. Geotherm. Res.*, *187*(3), 272–277.

Aoki, Y., M. Takeo, T. Ohminato, Y. Nagaoka, and K. Nishida (2013), Structural controls on magma pathways beneath Asama Volcano, Japan, *Geol. Soc. London Spec. Publ.*, *380*, 67–84.

Babuška, V., and M. Cara (1991), *Seismic Anisotropy in the Earth*, vol. 10, Springer, Dordrecht, Netherlands.

Bianco, F., M. Castellano, G. Milano, G. Ventura, and G. Vilardo (1998), The Somma–Vesuvius stress field induced by regional tectonics: Evidences from seismological and mesostructural data, *J. Volcanol. Geotherm. Res.*, *82*(1), 199–218.

Chapman, M., S. V. Zatsepin, and S. Crampin (2002), Derivation of a microstructural poroelastic model, *Geophys. J. Int.*, *151*(2), 427–451.

Christensen, N. I. (1996), Poisson's ratio and crustal seismology, *J. Geophys. Res.*, *101*(B2), 3139–3156.

Collet, O., and B. Gurevich (2013), Fluid dependence of anisotropy parameters in weakly anisotropic porous media, *Geophysics*, *78*(5), WC137–WC145.

Crampin, S. (1985), Evaluation of anisotropy by shear-wave splitting, *Geophysics*, *50*(1), 142–152.

Crampin, S. (1994), The fracture criticality of crustal rocks, *Geophys. J. Int.*, *118*(2), 428–438.

Del Negro, C., G. Currenti, and D. Scandura (2009), Temperature-dependent viscoelastic modeling of ground deformation: Application to Etna Volcano during the 1993–1997 inflation period, *Phys. Earth Planet. Inter.*, *172*(3), 299–309.

Fischer, K. M., E. Parmentier, A. R. Stine, and E. R. Wolf (2000), Modeling anisotropy and plate-driven flow in the Tonga subduction zone back arc, *J. Geophys. Res.*, *105*(B7), 16,181–16,191.

Gerst, A., and M. K. Savage (2004), Seismic anisotropy beneath Ruapehu Volcano: A possible eruption forecasting tool, *Science*, *306*(5701), 1543–1547.

Godfrey, N. J., N. I. Christensen, and D. A. Okaya (2000), Anisotropy of schists: Contribution of crustal anisotropy to active source seismic experiments and shear wave splitting observations, *J. Geophys. Res.*, *105*(B12), 27,991–28,007.
Grechka, V., and M. Kachang (2006), Effective elasticity of fractured rocks: A snapshot of the work in progress, *Geophysics*, *71*(6), W45–W58.
Gurevich, B., D. Makarynska, O. B. de Paula, and M. Pervukhina (2010), A simple model for squirt-flow dispersion and attenuation in fluid-saturated granular rocks, *Geophysics*, *75*(6), N109–N120.
Gurevich, B., M. Pervukhina, and D. Makarynska (2011), An analytic model for the stress-induced anisotropy of dry rocks, *Geophysics*, *76*(3), WA125–WA133.
Hudson, J. (1981), Wave speeds and attenuation of elastic waves in material containing cracks, *Geophys. J. R. Astron. Soc.*, *64*(1), 133–150.
Ji, S., A. Li, Q. Wang, C. Long, H. Wang, D. Marcotte, and M. Salisbury (2013), Seismic velocities, anisotropy, and shear-wave splitting of antigorite serpentinites and tectonic implications for subduction zones, *J. Geophys. Res. Solid Earth*, *118*, 1015–1037, doi:10.1002/jgrb.50110.
Johnson, J., and M. Poland (2013), Seismic detection of increased degassing before Kiluea's 2008 summit explosion, *Nat. Commun.*, *4*, 1668.
Johnson, J. H., S. Prejean, M. K. Savage, and J. Townend (2010), Anisotropy, repeating earthquakes, and seismicity associated with the 2008 eruption of Okmok Volcano, Alaska, *J. Geophys. Res.*, *115*, B00B04, doi:10.1029/2009JB006991.
Johnson, J. H., M. K. Savage, and J. Townend (2011), Distinguishing between stress-induced and structural anisotropy at Mount Ruapehu Volcano, New Zealand, *J. Geophys. Res.*, *116*, B12303, doi:10.1029/2011JB008308.
Jónsson, S. (2009), Stress interaction between magma accumulation and trapdoor faulting on Sierra Negra Volcano, Galápagos, *Tectonophysics*, *471*(1), 36–44.
Kazama, T., and S. Okubo (2009), Hydrological modeling of groundwater disturbances to observed gravity: Theory and application to Asama Volcano, Central Japan, *J. Geophys. Res.*, *114*, B08402, doi:10.1029/2009JB006391.
Kennett, B., E. Engdahl, and R. Buland (1995), Constraints on seismic velocities in the Earth from travel times, *Geophys. J. Int.*, *122*(1), 108–124.
McKenzie, D. P. (1969), The relation between fault plane solutions for earthquakes and the directions of the principal stresses, *Bull. Seismol. Soc. Am.*, *59*(2), 591–601.
Munson, C. G., C. H. Thurber, Y. Li, and P. G. Okubo (1995), Crustal shear wave anisotropy in Southern Hawaii: Spatial and temporal analysis, *J. Geophys. Res.*, *100*(B10), 20,367–20,377.
Murase, M., et al. (2007), Time-dependent model for volume changes in pressure sources at Asama Volcano, Central Japan due to vertical deformations detected by precise leveling during 1902–2005, *J. Volcanol. Geotherm. Res.*, *164*(1), 54–75.
Nagaoka, Y., K. Nishida, Y. Aoki, and M. Takeo (2010), Temporal change of phase velocity beneath Mt. Asama, Japan, inferred from coda wave interferometry, *Geophys. Res. Lett.*, *37*, L22311, doi:10.1029/2010GL045289.
Newman, A. V., T. H. Dixon, and N. Gourmelen (2006), A four-dimensional viscoelastic deformation model for Long Valley Caldera, California, between 1995 and 2000, *J. Volcanol. Geotherm. Res.*, *150*(1), 244–269.
Nur, A., and G. Simmons (1969), Stress-induced velocity anisotropy in rock: An experimental study, *J. Geophys. Res.*, *74*(27), 6667–6674.
Petrini, K., and Y. Podladchikov (2000), Lithospheric pressure-depth relationship in compressive regions of thickened crust, *J. Metamorph. Geol.*, *18*(1), 67–78.
Roman, D. C., and P. Heron (2007), Effect of regional tectonic setting on local fault response to episodes of volcanic activity, *Geophys. Res. Lett.*, *34*, L13310, doi:10.1029/2007GL030222.
Roman, D. C., M. K. Savage, R. Arnold, J. L. Latchman, and S. De Angelis (2011), Analysis and forward modeling of seismic anisotropy during the ongoing eruption of the Soufrière Hills Volcano, Montserrat, 1996–2007, *J. Geophys. Res.*, *116*, B03201, doi:10.1029/2010JB007667.
Savage, M. K., W. A. Peppin, and U. R. Vetter (1990), Shear wave anisotropy and stress direction in and near Long Valley Caldera, California, 1979–1988, *J. Geophys. Res.*, *95*(B7), 11,165–11,177.
Savage, M. K., T. Ohminato, Y. Aoki, H. Tsuji, and S. M. Greve (2010), Stress magnitude and its temporal variation at Mt. Asama Volcano, Japan, from seismic anisotropy and GPS, *Earth Planet. Sci. Lett.*, *290*(3), 403–414.
Sayers, C. M., and M. Kachang (1995), Microcrack-induced elastic wave anisotropy of brittle rocks, *J. Geophys. Res.*, *100*(B3), 4149–4156.
Sayers, C. M., and D.-H. M. Han (2002), The effect of pore fluid on the stress-dependent elastic wave velocities in sandstones, paper presented at the 2002 SEG Annual Meeting, Soc. of Explor. Geophys., Salt Lake City, Utah, 6–11 Oct.
Silver, P. G., and W. W. Chan (1991), Shear wave splitting and subcontinental mantle deformation, *J. Geophys. Res.*, *96*(B10), 16,429–16,454.
Taisne, B., S. Tait, and J. Claude (2011), Conditions for the arrest of a vertical propagating dyke, *Bull. Volcanol.*, *73*(2), 191–204.
Takagi, A., K. Fukui, K. Fujiwara, Y. Ueda, S. Iijima, T. Yamamoto, T. Sakai, T. Kanno, and H. Katayama (2005), Magma supply system of the 2004 eruption at Asama Volcano estimated by crustal deformation data, *Kazan*, *50*(5), 363–375.
Takeo, M., Y. Aoki, T. Ohminato, and M. Yamamoto (2006), Magma supply path beneath Mt. Asama Volcano, Japan, *Geophys. Res. Lett.*, *33*, L15310, doi:10.1029/2006GL026247.
Tanaka, H. K., T. Nakano, S. Takahashi, J. Yoshida, M. Takeo, J. Oikawa, T. Ohminato, Y. Aoki, E. Koyama, H. Tsuji, and K. Niwa (2007), High resolution imaging in the inhomogeneous crust with cosmic-ray muon radiography: The density structure below the volcanic crater floor of Mt. Asama, Japan, *Earth Planet. Sci. Lett.*, *263*(1), 104–113.
Townend, J., and M. D. Zoback (2006), Stress, strain, and mountain building in Central Japan, *J. Geophys. Res.*, *111*, B03411, doi:10.1029/2005JB003759.
Turcotte, D. L., and G. Schubert (2002), *Geodynamics*, Cambridge Univ. Press, New York.
Walsh, J. B. (1965), The effect of cracks on the compressibility of rock, *J. Geophys. Res.*, *70*(2), 381–389.
Wang, X.-Q., A. Schubnel, J. Fortin, E. C. David, Y. Guéguen, and H.-K. Ge (2012), High Vp/Vs ratio: Saturated cracks or anisotropy effects?, *Geophys. Res. Lett.*, *39*, L11307, doi:10.1029/2012GL051742.
Wookey, J. (2012), Direct probabilistic inversion of shear wave data for seismic anisotropy, *Geophys. J. Int.*, *189*(2), 1025–1037.
Zatsepin, S. V., and S. Crampin (1997), Modelling the compliance of crustal rock—I. Response of shear-wave splitting to differential stress, *Geophys. J. Int.*, *129*(3), 477–494.
Zinke, J. C., and M. D. Zoback (2000), Structure-related and stress-induced shear-wave velocity anisotropy: Observations from microearthquakes near the Calaveras Fault in Central California, *Bull. Seismol. Soc. Am.*, *90*(5), 1305–1312.